JOURNAL OF GEOPHYSICAL RESEARCH, VOL. 111, C06031, doi:10.1029/2005JC003398, 2006

The form of the asymptotic depth-limited wind wave frequency spectrum

I. R. Young[1] and A. V. Babanin[1]

Received 17 November 2005; revised 9 January 2006; accepted 2 March 2006; published 24 June 2006.

[1] This paper presents a comprehensive set of field experiments investigating the form of the asymptotic, depth-limited wind wave frequency spectrum. Such a spectrum represents the upper limit to growth from active wind forcing in finite depth conditions. The data clearly define asymptotic limits for the nondimensional energy and nondimensional wave number as functions of nondimensional water depth. In contrast to deep water spectra, the asymptotic depth-limited form has a harmonic at a frequency slightly less than twice the spectral peak frequency. A parametric form is proposed for the spectral form, and clear functional relationships are found for all the spectral parameters. These relationships mean that the full asymptotic, depth-limited spectrum can be determined with knowledge of only the water depth and wind speed.

Citation: Young, I. R., and A. V. Babanin (2006), The form of the asymptotic depth-limited wind wave frequency spectrum, *J. Geophys. Res.*, *111*, C06031, doi:10.1029/2005JC003398.

1. Introduction

[2] Determination of the form of the one-dimensional (or omnidirectional) surface gravity wave spectrum in water of finite depth is important for many scientific and engineering applications. In particular, the asymptotic form of the spectrum which would result if the wind blows over a body of uniform finite depth water for an infinite (or sufficiently long) period of time is an important result. This spectral form specifies the extreme case for coastal design or sediment transfer studies. Determination of this spectral form also provides an invaluable limiting form for the testing of finite depth numerical wave models as well as shedding additional insight on the physical processes active in such situations.

[3] Despite the importance of this limiting form, there are almost no reliable field measurements of this quantity. Those which are available do not define the spectrum or the environmental conditions to the degree of accuracy desirable. In most cases, the finite depth form is not independently derived, but extrapolated from parametric forms applicable in deep water (e.g., JONSWAP) [*Hasselmann et al.*, 1973]. More recent studies now question the applicability of these deep water forms [e.g., *Toba*, 1973; *Kawai et al.*, 1977; *Mitsuyasu et al.*, 1980; *Kahma*, 1981; *Forristall*, 1981; *Donelan et al.*, 1985; *Zakharov*, 2005].

[4] This study addresses these concerns by presenting detailed measurements of the finite depth spectral form under cases of extreme forcing, where the spectra have reached a state of fully developed equilibrium, limited by the water depth. The instrumentation is such that the wind speed, water depth and frequency resolution are all known to high accuracy. On the basis of this data, it is possible to accurately define the depth asymptotes for nondimensional energy and nondimensional peak frequency. In addition, it is possible to define the limiting form of the one-dimensional spectrum and to present this in a parametric form, suitable for a wide range of applications.

[5] The arrangement of the paper is as follows. Section 2 presents an overview of previous studies of finite depth wind wave spectra. Section 3 describes the field study, instrumentation and data collected for this study. This is followed by an analysis of the limiting values of the integral parameters of nondimensional energy and nondimensional peak frequency in section 4. Section 5 discusses the limiting form of the one-dimensional spectrum and presents a parametric representation of the spectrum. Conclusions and discussion of the results are made in section 6. In addition, two appendices are included: these include an error analysis for the data and examples of the predictive capability of the parametric form of the spectrum proposed in this study.

2. Depth-Limited Spectral Investigations

[6] Numerous deep water studies of wind wave growth have attempted to represent fetch-limited growth in terms of the nondimensional variables: nondimensional energy $\varepsilon = g^2E/U_{10}^4$, nondimensional peak frequency $\nu = f_pU_{10}/g$ and nondimensional fetch $\chi = gx/U_{10}^2$. In these relationships: g is gravitational acceleration, E is the total wave energy or variance, f_p is the spectral peak frequency, x is the fetch and U_{10} is the wind speed measured at a reference height of 10 m. Debate still exists over whether U_{10} is the most appropriate scaling parameter for the wind speed, with the friction velocity $u*$ and the velocity measured at one half wavelength above the surface $U_{\lambda/2}$ proposed as alternatives. The various studies show significant scatter in the data

[1]Faculty of Engineering and Industrial Sciences, Swinburne University of Technology, Melbourne, Victoria, Australia.

0148-0227/06/2005JC003398$09.00

(*Battjes et al.* [1987] and *Kahma and Calkoen* [1992] amongst many studies) but clear relationships between the nondimensional variables do exist.

[7] In the analysis which follows, U_{10} is adopted as the scaling wind speed. This choice is made for pragmatic reasons, rather than any evidence that U_{10} is better or worse than the other wind speed choices. In our case, measurements were made of the full atmospheric boundary layer and hence both $u*$ and $U_{\lambda/2}$ could be determined. A major aim of this study is to develop a spectral formulation generally applicable in finite depth conditions. In such cases, U_{10} is usually the only wind speed measure available. The determination of either $u*$ or $U_{\lambda/2}$ would require an assumed value for the surface drag coefficient. There is an ongoing debate about the most appropriate formulation for the drag coefficient in deep water. Data defining the drag coefficient in finite depth conditions is extremely rare and appropriate formulations do not exist. Indeed, preliminary analysis of data obtained at Lake George indicates that the drag coefficient is larger than in commensurate deep water situations. Hence, in order to avoid introducing further uncertainties, U_{10} has been adopted as the scaling wind speed.

[8] For finite depth conditions, the wind wave data set is much more limited than in deep water. Many measurements exist of waves in complex shoaling conditions, but comparatively few in fetch-limited and/or constant finite depth situations under active wind forcing. The first study of finite depth wave growth was conducted by *Thijsse* [1949]. This was followed by the field investigations in Lake Okeechobe, USA [*U.S. Army Corps of Engineers*, 1955; *Bretschneider*, 1958]. The Lake Okeechobe study was limited by the instrumentation and recording techniques of the time (paper tape etc.) and concentrated on determining the asymptotic limits to growth, rather than on an understanding of fetch-limited evolution. *Ijima and Tang* [1966] combined these limiting values with a numerical model study to develop fetch-limited formulations, later reproduced for engineering design in *Coastal Engineering Research Center* [1984].

[9] In the only really detailed study of this form of growth, *Young and Verhagen* [1996a] compiled an extensive fetch-limited finite depth data set from Lake George, Australia. They developed parametric forms for the fetch-limited growth of the nondimensional quantities, ε and ν, as well as asymptotic depth-limited forms for these quantities (these asymptotic values are represents here by ε_d and ν_d, respectively):

$$\varepsilon_d = 1.06 \times 10^{-3} \delta^{1.3} \tag{1}$$

$$\nu_d = 0.20 \delta^{-0.375} \tag{2}$$

In the above, $\delta = gd/U_{10}^2$ is termed the nondimensional water depth and d is the depth. Observations of finite depth wind wave spectra (as opposed to shoaling waves) are similarly limited. *Bouws et al.* [1985, 1987] considered the so-called TMA data set, comprising measurements made at three coastal sites (TEXEL –Dutch North Sea; MARSEN – German Bight; ARSLOE – U.S. East coast). Following *Kitaigorodskii* [1962] and *Kitaigorodskii et al.* [1975] they assumed a wave number spectrum of the form

$$Q(k) = \frac{\alpha}{2} k^{-3} \Psi\left(k, f_p, d\right) \tag{3}$$

where α is a scale parameter, k is the modulus of the wave number vector $k = |\underline{k}|$ and Ψ is a nondimensional shape function which approaches unity for $k \gg k_p$, where k_p is the wave number of the spectral peak. Converting (3) to a frequency spectrum, assuming linear wave theory, results in a form proportional to f^{-5} in deep water and f^{-3} for shallow water (i.e., nondispersive waves). *Bouws et al.* [1985] assumed a shape function of the JONSWAP form [*Hasselmann et al.*, 1973], resulting in the TMA spectral form

$$F(f) = \alpha g^2 (2\pi)^{-4} f^{-5} \exp\left[-\frac{5}{4}\left(\frac{f}{f_p}\right)^{-4}\right] \gamma^{\exp\left[\frac{-(f-f_p)^2}{2\sigma^2 f_p^2}\right]} \Phi \tag{4}$$

where

$$\Phi = \left\{ \frac{[k(f,d)]^{-3} \frac{\partial k(f,d)}{\partial f}}{[k(f,\infty)]^{-3} \frac{\partial k(f,\infty)}{\partial f}} \right\} \tag{5}$$

By neglecting the shape function in (3), *Bouws et al.* [1985] approximated the total spectral energy as

$$E = \int_0^\infty Q(k) dk \approx \frac{\alpha}{2} \int_{k_p}^\infty k^{-3} dk \tag{6}$$

Introducing nondimensional variables, (6) yields

$$\varepsilon = \frac{\alpha}{4} \kappa^{-2} \tag{7}$$

where $\kappa = U_{10}^2 \; k_p/g$ is the nondimensional peak wave number. *Bouws et al.* [1985] found that (7) was a reasonable approximation to their data set. They further examined the spectral parameters defining (4) and found that α was an increasing function of κ, although there was significant scatter in the data. Consistent with previous deep water studies, they could find no dependence for the parameters γ and σ.

[10] The TMA formulation is predicated on a wave number spectral form proportional to k^{-3} (deep water frequency spectrum proportional to f^{-5}). Numerous deep water studies [*Toba*, 1973; *Kawai et al.*, 1977; *Mitsuyasu et al.*, 1980; *Kahma*, 1981; *Forristall*, 1981; *Donelan et al.*, 1985] have indicated that a better approximation to the deep water frequency spectrum is a form proportional to f^{-4}. *Miller and Vincent* [1990] adopted this form, which transforms to a wave number spectrum proportional to $k^{-2.5}$, finding that it modeled recorded data equally as well as the TMA form.

[11] *Young and Verhagen* [1996b] examined the finite depth spectra from their Lake George study, finding that there was considerable variability in the exponent, n, defining the high-frequency spectral face of the form, f^n.

Within the data scatter, there was some indication that the value of n decreased from -5 (or -4) in deep water to numerically smaller values in finite depth conditions. Such a result is consistent with the wave number scaling arguments of *Kitaigorodskii et al.* [1975], as represented, for example, in (3). Either form (k^{-3} or $k^{-2.5}$) could have equally been used to approximate the *Young and Verhagen* [1996b] data. They adopted the TMA form ($\sim k^{-3}$), modifying (7) to obtain the best fit to the data as

$$\varepsilon = 0.14\left(\alpha\kappa^{-2}\right)^{0.91} \tag{8}$$

The spectral parameter α was represented as

$$\alpha = 0.0091\kappa^{0.24} \tag{9}$$

which is consistent with the result of *Bouws et al.* [1985]. Again, they could find no trend for the parameters γ or σ.

[12] *Young and Verhagen* [1996b] argued that the difficulties in defining these spectral parameters were due to the statistical variability of the spectral estimates and the relatively course frequency resolution of the spectra. Although estimates of spectra, obtained from finite length time series are notoriously noisy, the data scatter may also be due to limitation of the adopted spectral form.

[13] Spectral forms, such as (3) or (4) are extrapolations of deep water formulations and hence there is an implicit assumption that the physics governing spectral evolution is similar in both cases. In deep water, it is generally accepted that the spectrum evolves because of the balance between atmospheric input, nonlinear interaction and whitecap dissipation [*Komen et al.*, 1994], with the nonlinear term having a dominant role in determining the spectral shape [*Young and van Vledder*, 1993; *Zakharov*, 2005]. In finite depth conditions, the spectral balance is similar, with an additional term to represent decay due to bottom friction. All the source terms change form in finite depth conditions, but not to the extent that the general form of the spectrum is likely to deviate markedly from the deep water form. As water depth decreases, triad, or three wave interactions become increasingly important [*Beji and Battjes*, 1993; *Eldeberky and Battjes*, 1995]. Such interactions generate harmonics of the spectral peak and are likely to cause the depth-limited spectrum to deviate from the deep water spectral form. Indeed, *Young and Eldeberky* [1998] used bispectral analysis to show significant influence of triad interactions in the Lake George data and the development of a clear harmonic at $2f_p$. Such changes in the spectral form may limit the applicability of forms such as (4), and account for some of the scatter in the spectral parameters.

[14] None of these previous studies have attempted to define the asymptotic limiting form of the wind-generated spectrum in finite depth water, although such spectra clearly existed in both the Lake Okeechobe and Lake George data sets. It is likely that for such limiting forms, triad interactions will be important and that the deep water extrapolated forms, represented by relationships such as (4) will have only limited applicability.

[15] Determination of the detailed shape of the finite depth spectrum has practical significance. Numerical modeling of waves in the nearshore zone has consistently encountered difficulties in reproducing measurements. If the models are tuned to produce correct wave heights, discrepancies are often observed with respect to wave periods [e.g., *Tozer et al.*, 2005]. It is not clear whether the discrepancies are due to the wave model or the nearshore measurements. Accurately measured and parameterized, rather than inferred, finite depth wave spectra may be able to address this issue.

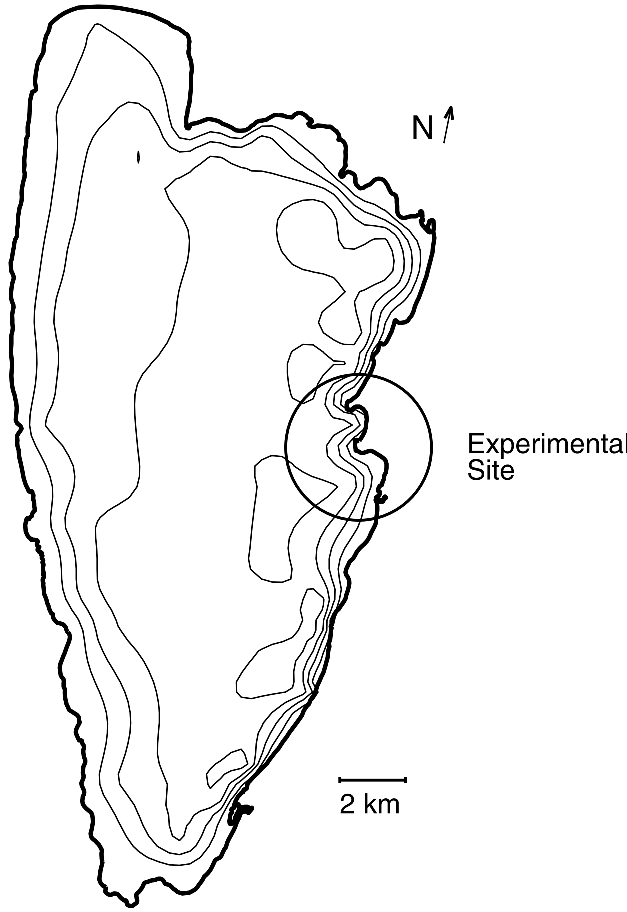

Figure 1. Contour plot of Lake George in southeastern Australia. The experimental site on the eastern shore of the lake is shown. The water level varies seasonally, with the contour interval 0.5 m.

3. Experimental Configuration and Recorded Data

[16] The experimental site was Lake George in southeastern Australia. The lake has been well documented in the finite depth studies of *Young and Verhagen* [1996a, 1996b] and *Young et al.* [1996]. The lake and the location of the experimental site are shown in Figure 1. When full, the lake is approximately 20 km long and 10 km wide, with a water depth of approximately 2.5 m. The present experiments were conducted when the lake was at a relatively low level, with the water depth at the measurement site ranging between 1.15 m and 0.40 m. The lake bed has been built up from fine grained silt laid down over many thousands of years. As a result, the bed is quite uniform and relatively

horizontal. The bed slopes toward the eastern side (measurement location) with a bed slope of approximately 1×10^{-4}. For practical purposes, it can be regarded as horizontal and constant depth.

[17] The experimental location consisted of a shore-connected platform, approximately 50 m offshore and outside the "surf" zone. The location enabled measurements to be made over an extended period of time and over a range of water depths. Records of water surface elevation were made using an array of capacitance wave probes (see *Young et al.* [2005] for details). The array was located midway along a 10 m measurement bridge extending from the platform. The data analysis described in this paper, used only a single probe. The probes consisted of Teflon coated wires, 1 m long and 1 mm in diameter. The probes and associated electronics were provided by Richard Brancker Research Ltd., Canada. Manufacturing specifications indicated 0.2% linearity, 0.4% accuracy and a 2 ms response time. Detailed static and dynamic calibrations of the probes were performed in the laboratory prior to deployment. These tests confirmed the linearity and dynamic response of the probes. The array was removed from the water at the start and finish of each day and a static calibration performed on site. These repeated calibrations indicated that the probes were remarkably stable and a single linear calibration relationship has been used for all data analysis. The wave probes were sampled at 25 Hz, with individual records of 20 min duration (i.e., 30,000 samples). These records were processed to obtain one-dimensional spectra. These spectra were formed by subdividing the time series into blocks of 256 points and ensemble averaging the resulting spectra of these blocks to yield a final spectrum with approximately 230 degrees of freedom and a Nyquist frequency of 12.5 Hz.

[18] Wind records were measured from two anemometer masts. The first was erected at the end of the measurement bridge and contained cup anemometers at nominal heights of 10 m and 5.65 m and a direction vane at a height of 10 m. A second mast was erected a further 6m from the end of the measurement bridge and contained four further cup anemometers and one direction vane at heights below 5 m. This mast was found necessary as initial measurements indicated disturbance of the air flow at lower heights due to the proximity of the platform and the bridge. In total, the wind profile was measured at six heights, logarithmically placed from 10 m down to 22 cm above the mean water level. The wind direction was measured at 10 m and 0.89 m. As the water level varied over the period of the measurements, the measured boundary layer profiles were used to determine the wind speed at an elevation of 10 m for each measured time series.

[19] The wind sensors were Aanderaa Instruments Wind Speed Sensor 2740 and Wind Direction Sensor 3590. The wind speed sensor consisted of a three cup rotor with a threshold speed less than 0.4 m/s, an accuracy of ±2% or ±0.2 m/s, whichever is greater. The wind direction vane had a threshold speed of 0.3 m/s and an accuracy of ±5°. The sensor outputs consisted of 1-min average values. These 1-min values were averaged to obtain representative wind speed and direction values for the 20-min wave records. The platform, measurement bridge and associated instrumentation are shown in Figure 2.

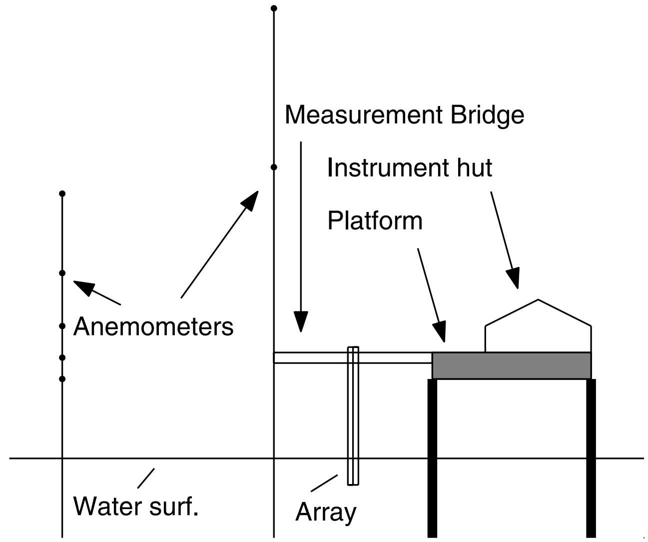

Figure 2. Diagram showing the measurement structure. Measurements were made using a capacitance probe array in the center of the measurement bridge. Wind data were recorded from the anemometer masts at the end of the measurement bridge.

[20] The water depth was recorded manually for each record using a "stilling" pipe which filtered out wave oscillations.

[21] Data were recorded over a period of approximately 1 year between September 1997 and October 1998. A full summary of the 92 wave records making up the data set is contained in Table 1. Only records for which the wind direction was between 260° and 300° were retained, thus ensuring that the wind direction was onshore (see Figure 1). (Note that the nautical wind direction convention is used; that is, winds from the west are at 270°). The walkway was constructed from the end of southern point shown in the position circle of Figure 1. Thus the accepted range of wind directions ensured contamination by lateral boundary conditions was negligible. At low wind speeds, both the magnitude and direction of the wind tend to vary significantly during the 20 min records. Therefore all records with $U_{10} < 5$ m/s were excluded. The resulting data in Table 1 span 5.6 m/s $< U_{10} <$ 19.8 m/s. The data set contains water depths in the range 0.6 m $< d <$ 1.15 m and nondimensional depth, $k_p d$ in the range $0.71 < k_p d < 3.5$. Noting that deep water conditions are usually assumed for $k_p d > \pi$ and shallow water conditions for $k_p d < \pi/10$, the present data set spans most of the transitional water depth region. As indicated by *Young and Verhagen* [1996a] and supported by this data set, it is unlikely that wind generated seas (as opposed to shoaling waves) ever become shallow water waves, in this sense (i.e., $k_p d < \pi/10$), their evolution being halted by finite depth effects (bottom friction and breaking) before they reach such small vales of $k_p d$.

4. Depth-Limiting Values of Total Energy and Peak Frequency

[22] On the basis of their extensive data set, *Young and Verhagen* [1996a] investigated the limiting values of non-

Table 1. Summary of All Data Collected[a]

	Date[b]	δ	ε	κ	H_s, m	f_p, Hz	U_{10}, m/s	d, m	k_pd	U_r	F_c	Depth Flag
1	c010204.no7	4.86e-002	2.13e-005	17.11	0.338	0.398	13.400	0.89	0.832	21.7	124	1
2	c010226.no7	4.57e-002	2.25e-005	17.93	0.374	0.391	13.900	0.90	0.819	24.4	134	1
3	c010248.no7	4.17e-002	1.93e-005	19.97	0.392	0.389	14.800	0.93	0.832	24.0	131	1
4	c010716.no7	7.67e-002	3.24e-005	11.84	0.318	0.390	11.700	1.07	0.908	14.2	91.7	0
5	c010739.no7	7.24e-002	3.19e-005	12.66	0.337	0.391	12.100	1.08	0.916	14.7	92.3	1
6	c010803.no7	6.06e-002	2.11e-005	16.05	0.322	0.413	13.100	1.06	0.973	12.7	80.9	0
7	c010827.no7	6.08e-002	2.24e-005	15.86	0.337	0.407	13.200	1.08	0.964	13.2	83.4	0
8	c010849.no7	7.41e-002	3.44e-005	12.73	0.339	0.402	11.900	1.07	0.944	14.0	87.7	1
9	c011210.oc8	1.15e-001	4.97e-005	9.90	0.233	0.493	9.000	0.95	1.14	7.45	53.8	0
10	c011245.oc8	9.51e-002	4.28e-005	10.45	0.261	0.444	9.900	0.95	0.994	11.0	73.9	0
11	c011323.oc8	8.96e-002	5.09e-005	10.21	0.303	0.416	10.200	0.95	0.915	15.0	93.6	1
12	c011406.oc8	7.56e-002	3.49e-005	12.18	0.297	0.418	11.100	0.95	0.921	14.5	91.5	1
13	c011445.oc8	5.43e-002	2.13e-005	15.70	0.323	0.393	13.100	0.95	0.852	18.5	112	0
14	c021217.ja8	1.20e-001	1.72e-005	19.52	0.083	0.976	7.000	0.60	2.34	0.991	13	0
15	c021332.ja8	1.58e-001	1.65e-005	17.76	0.062	1.074	6.100	0.60	2.81	0.513	8.81	0
16	c021414.ja8	1.64e-001	2.36e-005	15.84	0.071	1.029	6.000	0.60	2.59	0.70	10.5	0
17	c031151.se8	2.78e-001	1.62e-004	5.42	0.169	0.607	5.700	0.92	1.50	3.20	28.7	1
18	c031211.oc7	6.01e-002	3.20e-005	15.54	0.433	0.384	13.700	1.15	0.934	17.00	97.7	1
19	c031214.se8	2.35e-001	1.19e-004	5.89	0.171	0.574	6.200	0.92	1.38	3.84	33.3	0
20	c031233.oc7	6.10e-002	2.69e-005	15.06	0.391	0.379	13.600	1.15	0.918	15.9	96	1
21	c031243.se8	2.56e-001	1.25e-004	5.55	0.159	0.589	5.900	0.91	1.42	3.41	30.7	0
22	c031253.oc7	6.28e-002	3.40e-005	15.02	0.427	0.388	13.400	1.15	0.944	16.5	95	1
23	c031307.se8	2.01e-001	1.15e-004	6.78	0.196	0.569	6.700	0.92	1.36	4.53	36.5	1
24	c031310.oc7	7.11e-002	3.79e-005	13.40	0.398	0.390	12.600	1.15	0.952	15.1	90.2	1
25	c031327.oc7	6.47e-002	3.50e-005	14.69	0.420	0.390	13.200	1.15	0.951	15.9	92.8	1
26	c031331.se8	1.16e-001	5.27e-005	9.98	0.234	0.502	8.900	0.94	1.16	7.29	52.3	0
27	c031347.oc7	6.89e-002	3.10e-005	14.05	0.372	0.395	12.800	1.15	0.967	13.6	84.5	1
28	c031356.se8	1.64e-001	1.13e-004	7.06	0.243	0.501	7.500	0.94	1.16	7.64	53.8	1
29	c031407.oc7	5.84e-002	2.77e-005	15.23	0.414	0.370	13.900	1.15	0.889	18	105	1
30	c031419.se8	2.51e-001	1.76e-004	4.76	0.195	0.518	6.000	0.92	1.19	5.88	46	1
31	c031427.oc7	6.28e-002	3.11e-005	14.48	0.409	0.377	13.400	1.15	0.91	16.9	99.9	1
32	c031442.se8	2.75e-001	1.96e-004	4.54	0.185	0.537	5.700	0.91	1.25	5.16	41.6	1
33	c041511.se7	3.57e-001	3.50e-005	9.76	0.073	0.886	5.500	1.10	3.48	0.216	5.38	0
34	c061151.oc8	5.46e-002	2.21e-005	16.56	0.334	0.408	13.200	0.97	0.905	16.6	99.6	0
35	c061234.oc8	6.09e-002	2.14e-005	15.29	0.294	0.417	12.500	0.97	0.931	13.8	88.2	0
36	c061323.oc8	5.38e-002	2.18e-005	16.71	0.336	0.406	13.300	0.97	0.899	16.9	101	0
37	c061425.oc8	5.07e-002	1.99e-005	16.74	0.341	0.387	13.700	0.97	0.849	19.3	114	0
38	c081352.se7	5.67e-002	3.14e-005	14.08	0.435	0.346	13.800	1.10	0.798	24.6	138	1
39	c111051.oc7	6.72e-002	1.66e-005	28.16	0.276	0.628	12.900	1.14	1.89	2.67	23.2	0
40	c111124.oc7	6.83e-002	1.77e-005	27.78	0.281	0.629	12.800	1.14	1.90	2.71	23.3	0
41	c111156.oc7	7.04e-002	1.87e-005	24.56	0.280	0.596	12.600	1.14	1.73	3.24	26.7	0
42	c111224.oc7	7.90e-002	2.02e-005	23.46	0.259	0.620	11.900	1.14	1.85	2.62	23.2	0
43	c111402.oc7	6.62e-002	1.62e-005	27.30	0.277	0.611	13.000	1.14	1.81	2.94	24.9	0
44	c111538.oc7	8.31e-002	2.09e-005	23.95	0.251	0.647	11.600	1.14	1.99	2.19	20.6	0
45	c141215.no7	5.69e-002	2.47e-005	14.08	0.343	0.367	13.000	0.98	0.801	21.5	129	1
46	c141215.oc7	1.05e-001	1.78e-005	24.28	0.175	0.757	10.100	1.09	2.54	0.981	12.6	0
47	c141237.no7	6.68e-002	2.72e-005	13.10	0.306	0.395	12.000	0.98	0.875	16.1	102	0
48	c141250.oc7	8.84e-002	1.59e-005	27.76	0.197	0.742	11.000	1.09	2.45	1.18	14	0
49	c141259.se8	9.14e-002	3.11e-005	13.32	0.232	0.517	10.100	0.95	1.22	6.51	47.6	0
50	c141305.no7	4.93e-002	1.82e-005	18.06	0.346	0.397	14.100	1.00	0.891	17.2	103	0
51	c141328.no7	4.89e-002	1.82e-005	17.60	0.356	0.382	14.300	1.02	0.861	18.6	111	0
52	c141351.no7	4.85e-002	1.95e-005	18.13	0.379	0.385	14.500	1.04	0.88	18.6	108	1
53	c141358.se8	8.29e-002	2.89e-005	13.73	0.246	0.492	10.600	0.95	1.14	7.88	55.4	0
54	c141415.no7	4.29e-002	1.37e-005	19.86	0.362	0.373	15.500	1.05	0.851	18.8	113	0
55	c141448.se8	1.08e-001	3.39e-005	13.23	0.205	0.577	9.300	0.95	1.43	4.2	34.1	0
56	c141502.se8	9.90e-002	3.44e-005	11.62	0.225	0.496	9.700	0.95	1.15	7.06	51.9	0
57	c151238.de7	6.53e-002	1.69e-005	17.05	0.207	0.521	11.100	0.82	1.11	8.03	57	0
58	c151249.se7	1.10e-001	6.88e-005	9.16	0.331	0.417	9.900	1.10	1.01	11.7	75.2	1
59	c151301.de7	5.92e-002	1.59e-005	15.82	0.227	0.451	11.800	0.84	0.936	12.2	82.3	0
60	c151325.de7	5.99e-002	1.87e-005	15.19	0.245	0.438	11.800	0.85	0.91	13.8	90.1	0
61	c151342.se7	1.30e-001	6.92e-005	8.97	0.281	0.466	9.100	1.10	1.17	7.38	52.4	1
62	c151405.de7	5.23e-002	1.50e-005	17.19	0.243	0.442	12.400	0.82	0.899	14.4	93.4	0
63	c151410.se7	1.15e-001	6.09e-005	9.80	0.299	0.453	9.700	1.10	1.12	8.5	58.1	1
64	c161149.se8	1.37e-001	4.91e-005	11.41	0.192	0.616	8.200	0.94	1.56	3.3	28.5	0
65	c161318.se8	1.16e-001	4.23e-005	12.69	0.210	0.594	8.900	0.94	1.48	4.05	32.7	0
66	c161425.de7	1.46e-001	2.21e-005	19.47	0.091	0.994	6.900	0.71	2.85	0.626	9.69	0
67	c161454.oc7	1.06e-001	2.08e-005	21.54	0.179	0.732	9.800	1.04	2.29	1.3	15	0
68	c161507.de7	1.36e-001	2.28e-005	18.39	0.098	0.936	7.100	0.70	2.51	0.881	12	0
69	c191134.oc8	1.03e-001	1.85e-005	20.53	0.155	0.742	9.400	0.93	2.12	1.46	16.4	0
70	c191214.oc8	8.45e-002	1.48e-005	23.18	0.173	0.702	10.500	0.95	1.96	1.87	19.1	0
71	c191348.oc8	9.90e-002	1.73e-005	23.42	0.160	0.771	9.700	0.95	2.32	1.23	14.5	0
72	c201446.no7	1.94e-001	3.35e-005	17.61	0.106	0.976	6.700	0.89	3.43	0.401	7.36	0
73	c201532.no7	2.78e-001	4.63e-005	12.59	0.087	0.988	5.600	0.89	3.5	0.314	6.48	0

Table 1. (continued)

	Date[b]	δ	ε	κ	H_s, m	f_p, Hz	U_{10}, m/s	d, m	k_pd	U_r	F_c	Depth Flag
74	c211202.oc8	1.93e-001	2.38e-005	16.66	0.092	0.935	6.800	0.91	3.22	0.385	7.35	0
75	c211320.oc8	1.41e-001	2.32e-005	18.12	0.129	0.815	8.100	0.94	2.55	0.834	11.6	0
76	c221253.de7	7.15e-002	1.46e-005	24.21	0.150	0.760	9.800	0.70	1.73	2.82	24.9	0
77	c221421.de7	7.72e-002	1.54e-005	34.08	0.145	0.954	9.500	0.71	2.63	1.16	13.5	0
78	c261148.no7	2.37e-001	3.21e-005	10.84	0.080	0.866	5.900	0.84	2.57	0.573	9.58	0
79	c261219.no7	1.59e-001	2.53e-005	8.15	0.106	0.575	7.200	0.84	1.30	2.98	30.7	0
80	c261330.no7	1.26e-001	2.01e-005	8.96	0.120	0.519	8.100	0.84	1.12	4.45	42	0
81	c271100.oc7	2.50e-001	1.37e-004	5.06	0.178	0.532	6.100	0.95	1.27	4.59	38.8	0
82	c271235.oc7	1.53e-001	7.94e-005	7.66	0.221	0.503	7.800	0.95	1.17	6.67	49.7	1
83	c281153.se8	2.48e-001	1.68e-004	6.07	0.191	0.611	6.000	0.91	1.5	3.65	30.7	1
84	c281544.oc7	3.62e-001	1.91e-004	4.86	0.146	0.655	5.100	0.96	1.76	1.95	20.5	0
85	c311757.oc7	3.76e-002	9.79e-006	26.67	0.373	0.412	17.100	1.12	1.00	13.1	80	0
86	c311823.oc7	2.80e-002	9.92e-006	29.44	0.503	0.352	19.800	1.12	0.825	26.1	137	1
87	c311845.oc7	4.53e-002	2.40e-005	16.59	0.449	0.338	15.000	1.04	0.752	30.1	163	1
88	c311908.oc7	5.48e-002	3.32e-005	12.99	0.391	0.342	12.900	0.93	0.712	32.7	181	1
89	c311930.oc7	5.69e-002	2.97e-005	14.76	0.364	0.388	12.800	0.95	0.84	21.4	122	1
90	c311958.oc7	7.22e-002	4.19e-005	12.04	0.355	0.391	11.600	0.99	0.869	18.7	110	1
91	c312021.oc7	5.33e-002	3.00e-005	16.99	0.419	0.398	13.700	1.02	0.906	19.8	108	1
92	c312048.oc7	5.74e-002	3.53e-005	14.76	0.422	0.378	13.200	1.02	0.848	22.7	124	1

[a]Records with a value of 1 in the Depth Flag column define records classed as at the asymptotic depth limit, as defined in text.
[b]Dates are given in the format cddtttt.mmy, where dd is day, tttt is time, mm is month, and y is year (e.g., c312048.oc7 represents 31 October 1997 at time 2048).

dimensional energy, $\varepsilon = g^2E/U_{10}^4$ and nondimensional peak frequency, $\nu = f_pU_{10}/g$ as a function of the nondimensional water depth $\delta = gd/U_{10}^2$. The limiting values of ε and ν (ε_d and ν_d) are those which will be obtained in finite depth conditions, but at sufficiently long fetch and duration that these parameters are no longer important. As mentioned above (see (1) and (2)), *Young and Verhagen* [1996a] found asymptotic depth limits of $\varepsilon_d = 1.06 \times 10^{-3}\ \delta^{1.3}$ and $\nu_d = 0.20\delta^{-0.375}$.

[23] Figure 3a shows ε plotted as a function of δ and Figure 3b shows ν as a function of δ. Figures 3a and 3b show the original data of *Young and Verhagen* [1996a] and the present data set (i.e., Table 1). The present data overlap in parameter space with that of *Young and Verhagen* [1996a], but extend to smaller values of δ. Although the *Young and Verhagen* [1996a] data set is of high quality, one would generally expect the present data to be of even better quality. This data set was recorded with a much higher-resolution wave probe, with more refined measurements of the wind speed and under more closely observed environmental conditions (i.e., researchers were present for each of the observations).

[24] The data are broadly consistent with that of *Young and Verhagen* [1996a], but there are clear differences. The ε_d - δ relationship seems to increase a little more slowly than determined by *Young and Verhagen* [1996a]. A slight modification to the power law proposed by *Young and Verhagen* [1996a] fits both data sets well:

$$\varepsilon_d = 1.0 \times 10^{-3}\delta^{1.2} \tag{10}$$

The ν_d - δ relationship is, however, more difficult to reconcile. The present values of ν appear to be considerably below the asymptotic limit set by *Young and Verhagen* [1996a]. It is therefore interesting to investigate whether this form of relationship is most appropriate to represent the behavior of the spectral peak. Assuming linear wave theory is a reasonable approximation for the spectral peak of these intermediate depth waves, the dispersion relationship for the spectral peak is $\omega_p^2 = gk_p \tanh(k_pd)$. Introducing the nondimensional variables to this relationship yields

$$\nu^2 = \frac{(k_pd)\tanh(k_pd)}{4\pi^2}\delta^{-1} \tag{11}$$

Equation (11) indicates that constant values of k_pd will lie along power law relationships in ν - δ space. The present data support this relationship and (11) is shown in Figure 3b. As the slope of the family of curves defining (11) is significantly different to the asymptotic relationship of *Young and Verhagen* [1996a], the appropriateness of representing the limiting spectral peak value by ν_d may be questionable.

[25] An alternative may be to use the nondimensional wave number $\kappa = k_pU_{10}^2/g$ as the appropriate parameter. Figure 3c shows both data sets plotted in κ - δ space. An asymptotic limit is now clear (κ_d), which can be approximated by the relationship

$$\kappa_d = 1.80\delta^{-0.73} \tag{12}$$

Combining (10) and (12) yields the relationship

$$\varepsilon_d = 2.61 \times 10^{-3}\kappa_d^{-1.65} \tag{13}$$

It should be noted that (10), (12) and (13) hold for the asymptotic depth-limited case, rather than generally for any finite depth wind wave spectra.

[26] Although all of the present data set was recorded in water depths less than 1.2 m, not all of the data are at the asymptotic depth limit. As the aim of this paper is to determine the asymptotic form for the depth-limited spectrum, it is convenient to identify those records which approximately conform to this limit. Recognizing that there is statistical sampling variability associated with the data

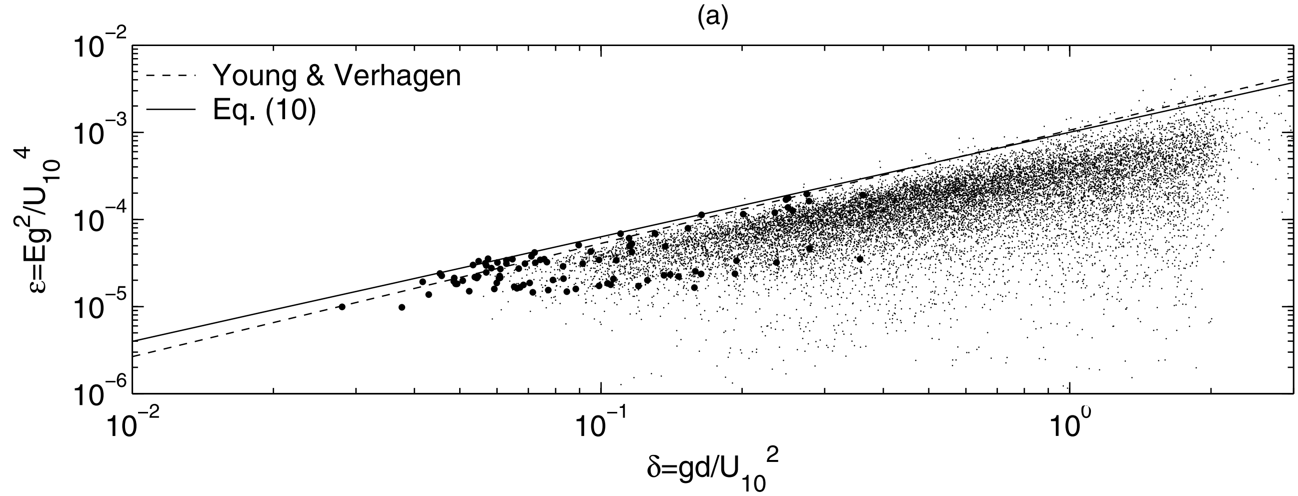

Figure 3a. Nondimensional energy, ε, as a function of the nondimensional water depth, δ. The data of *Young and Verhagen* [1996a] are shown by the small dots, and the present data are shown by the larger dots. Note that the full data set of Table 1 is shown. The asymptotic limit proposed by *Young and Verhagen* [1996a] is shown by the dashed line, and the modified limit (10) is shown as the solid line.

(see Appendix A), (10) and (12) were used to identified these records. Cases for which ε was within ±20 % of (10) and κ was within ±20 % of (13) were considered to be at the asymptotic depth limit. These records are shown in Table 1 with a depth flag set to 1. There are a total of 35 such records within the full data set.

5. Asymptotic Depth-Limited Frequency Spectrum

[27] Figures 4a and 4b show a typical spectrum from the present depth-limited data set. In comparison to deep water wind wave spectra, the obvious difference is the small harmonic which occurs at approximately $2f_p$. This is a feature of almost all of the spectra in the data set, whether they are at the asymptotic depth limit or not. In deep water, the unimodal spectral form with a high-frequency face of the form $F \propto f^n$ is generally assumed to be due to a balance between the processes of atmospheric input, nonlinear four-wave interactions and white cap dissipation. In the above, F is the variance spectrum (units of m^2 s), f is the frequency of the spectral component and n is an exponent. In finite depth water, the source term balance is more complex and includes all of the deep water processes plus nonlinear three-wave interactions and bottom friction. In deep water the four-wave nonlinear term plays a critical role in determining the detailed shape of the spectrum [*Hasselmann et al.*, 1973; *Young and van Vledder*, 1993]. The detailed spectral balance in finite depth water is not fully understood, although four-wave interactions are again expected to be

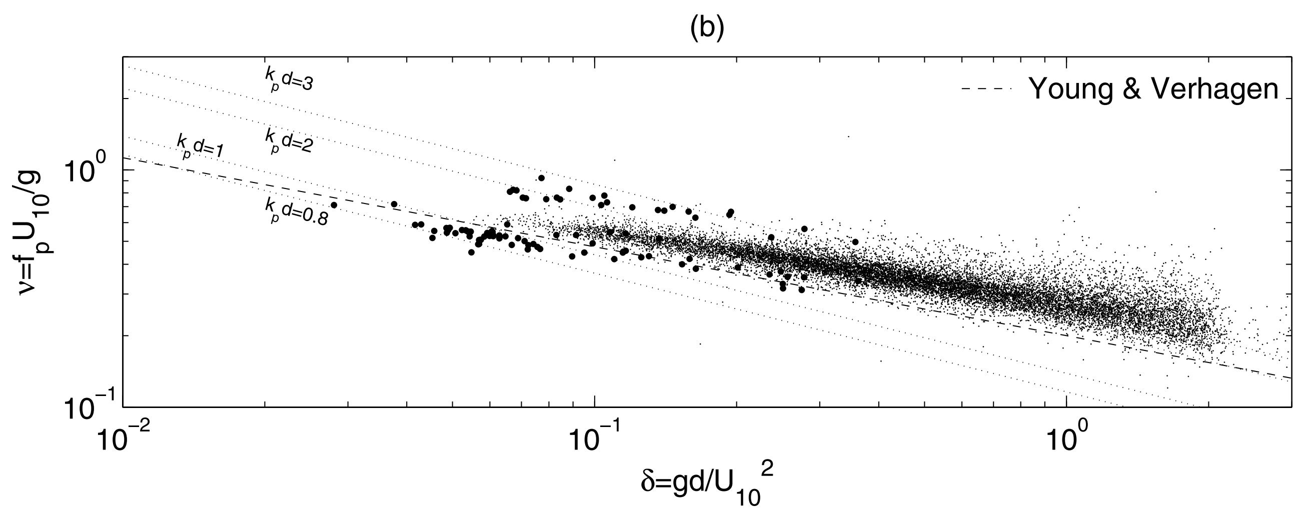

Figure 3b. Nondimensional frequency, ν, as a function of the nondimensional water depth, δ. The data of *Young and Verhagen* [1996a] are shown by the small dots, and the present data are shown by the larger dots. Note that the full data set of Table 1 is shown. The asymptotic limit proposed by *Young and Verhagen* [1996a] is shown by the dashed line. Lines of constant k_pd are shown by the dotted lines.

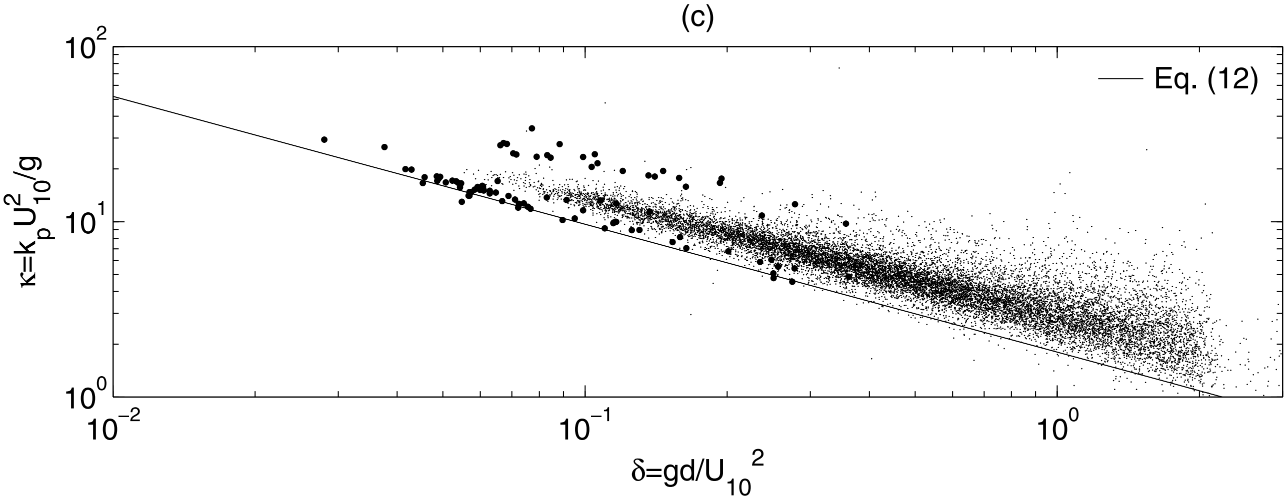

Figure 3c. Nondimensional wave number, κ, as a function of the nondimensional water depth, δ. The data of *Young and Verhagen* [1996a] are shown by the small dots, and the present data are shown by the larger dots. Note that the full data set of Table 1 is shown. The asymptotic limit defined by (12) is shown by the solid line.

important, especially since their relative magnitude increases in finite depth [*Hasselmann and Hasselmann*, 1985; *Young*, 1999]. In addition, three-wave (or triad) nonlinear interactions may become important in determining the finite depth spectral shape. Using bispectral analysis, *Young and Eldeberky* [1998] have shown strong triad coupling for finite depth spectra with similar values of $k_p d$ to the spectra discussed here. (Note that the *Young and Eldeberky* [1998] data were taken from Lake George). Reliable estimates of bispectra require estimates with extremely small confidence intervals. The *Young and Eldeberky* [1998] data are rare, in that they consider almost stationary time series many hours in length. Thus they are able to clearly show the triad coupling which occurs in these intermediate depth conditions. As none of the other known source terms can generate a harmonic of the form which exits in the present data and as the *Young and Eldeberky* [1998] data are clear, the existence of the harmonic is interpreted as a consequence of triad coupling in finite depth conditions.

5.1. Spectral Form

[28] Although the harmonic is relatively small, and in many cases manifests itself only as a change in slope of the spectrum, it significantly modifies the shape of the spectrum in the region immediately above the spectral peak. Since this region provides the major contribution to the zeroth and first moments of the spectrum, such modification may affect estimates of wave variance and mean frequency at finite depths, if these quantities are obtained by means of integrating a deep water-like spectrum with no harmonic.

[29] Because of the absence of the harmonic, typical unimodal spectral forms (e.g., *Hasselmann et al.* [1973] (JONSWAP), *Donelan et al.* [1985], and *Bouws et al.* [1987] (TMA)) represent a poor fit to the spectral shape. As a result, the following two-peak form was investigated

$$F = F_1 + F_2 \tag{14}$$

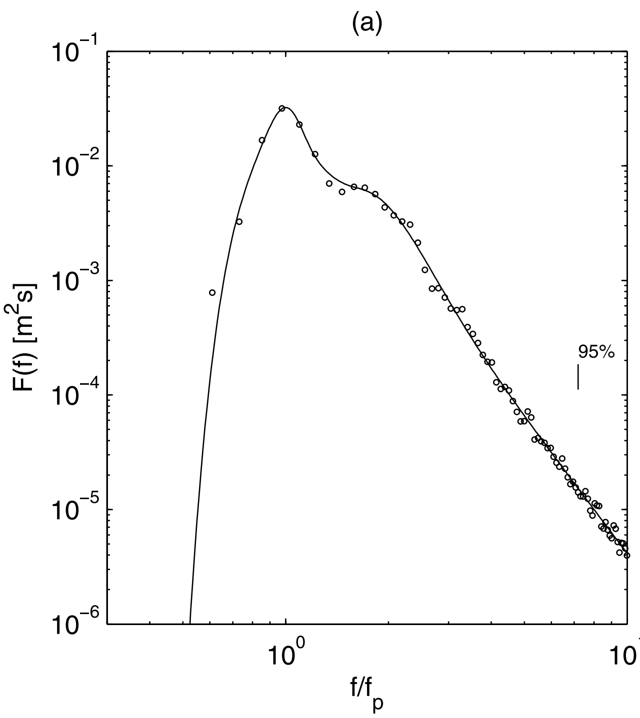

Figure 4a. Typical water surface elevation spectrum from the present data set. The case shown is c010204.no7, as detailed in Table 1. The spectral ordinates are shown by the open circles. The solid line shows the parametric fit to the data represented by (14). The 95% confidence interval for the individual spectral ordinates is shown by the short vertical line on the right. The spectrum is shown as a log-log plot.

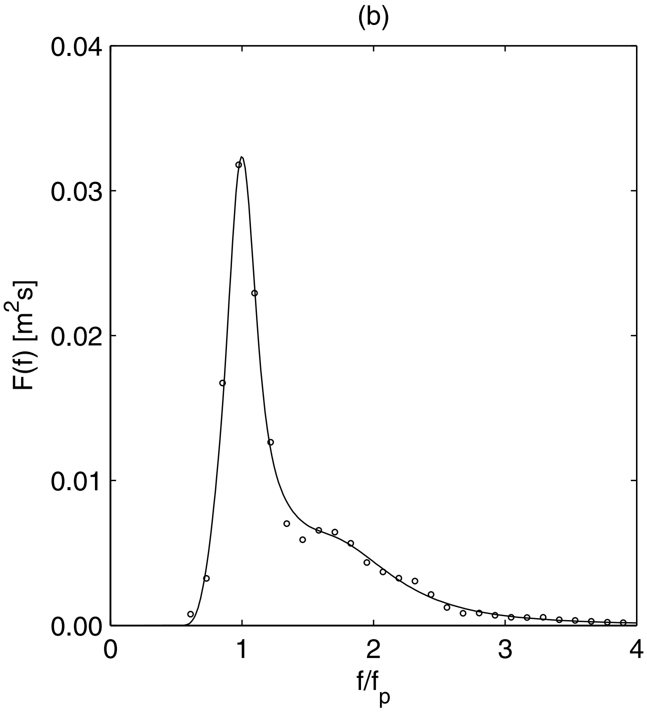

Figure 4b. As for Figure 4a but shown as a linear plot. The harmonic is still visible even in this presentation.

where

$$F_1(f) = \beta_1 g^2 (2\pi)^{-4} f_{p_1}^{-(5+n_1)} f^{n_1} \exp\left[\frac{n_1}{4}\left(\frac{f}{f_{p_1}}\right)^{-4}\right] \gamma_1^{\exp\left[\frac{-(f-f_{p_1})^2}{2\sigma_1^2 f_{p_1}^2}\right]} \tag{15}$$

$$F_2(f) = \beta_2 g^2 (2\pi)^{-4} f_{p_2}^{-(5+n_2)} f^{n_2} \exp\left[\frac{n_2}{4}\left(\frac{f}{f_{p_2}}\right)^{-4}\right] \tag{16}$$

Equations (14) to (16) define a two peaked form with peaks at f_{p_1} and f_{p_2} and with the high-frequency faces of the two superimposed spectra defined by exponents n_1 and n_2. In the present application, it is proposed that F_2 will approximate the harmonic. As this component is relatively small, the peak enhancement factor defined by γ has been neglected for this component of the spectrum.

[30] A range of spectral forms could have been chosen as alternatives to (15) and (16). An obvious choice would be to adopt a wave number formulation, rather than a frequency spectrum. Such formulations include those of *Bouws et al.* [1985], *Miller and Vincent* [1990], or *Smith and Vincent* [2002]. Selection of a wave number form for the spectrum seems logical, in light of the wave number scaling adopted for the asymptotic limit (12). The present data set was, however, obtained from time series observations of the water surface elevation, from which frequency spectra can be directly determined. Evaluation of wave number spectra would require the application of an assumed (probably linear) dispersion relationship. This was deemed appropriate at the peak of the spectrum for the evaluation of (12). The existence of the harmonic in the spectra indicates that nonlinear process are active and it is highly likely that the high-frequency components of the spectrum will be impacted by this nonlinear coupling to the spectral peak. Hence determination of the wave number spectrum from the frequency spectrum is not a straightforward process. Because of the potential uncertainties, investigation of an inferred wave number spectrum has not been considered.

[31] Equations (15) and (16) were preferred over more typical deep water forms [*Hasselmann et al.*, 1973; *Donelan et al.*, 1985] with a fixed high-frequency exponent n, as it provides greater flexibility and the opportunity to investigate the behavior of this exponent in finite depth conditions.

[32] Equations (14) to (16) contain 8 fitting parameters. The summation form (14) was fitted to all of the spectra in Table 1. The parameters were determined for each spectrum using a Levenberg-Marquardt nonlinear regression model [*Levenberg*, 1944]. This spectral form proved a remarkably reliable approximation to the measured spectra, an example appearing in Figures 4a and 4b.

5.2. Development of the Spectral Peak Harmonic

[33] The harmonic of the spectral peak is a clear finite depth characteristic of the spectra of the present data set, irrespective of whether the spectra were at the asymptotic depth limit, or not. As a result, it was important to investigate the generation of this harmonic. As the generation of the harmonic can be associated with three-wave nonlinear interactions, it might be expected that the magnitude of the harmonic would be associated with the degree of nonlinearity of the wave record. A typical measure of finite depth wave nonlinearity is the Ursell parameter, here defined as $U_r = H_s L_p^2/d^3$, where $H_s = 4\sqrt{E}$ is the significant wave height and $L_p = 2\pi/k_p$ is the wavelength of the waves at the spectral peak.

[34] The magnitude of the harmonic can be represented by determining the ratios of the total energies contained in the two components of the spectrum (14), $R = E_2/(E_1 + E_2)$, where $E_1 = \int F_1(f)df$ and similarly for E_2. The ratio R is shown in Figure 5 as a function of the Ursell parameter, U_r. There appears to be no correlation between the magnitude of the energy in the harmonic and the degree of nonlinearity, even though U_r ranges over 2 orders of magnitude from 0.3 (linear) to 30 (nonlinear). Alternative measures of nonlinearity were also investigated, including the parameter $F_c = \left(\frac{H_s}{d}\right)^{1/2} \left[T_p\sqrt{\frac{g}{d}}\right]^{5/2}$ proposed by *Nelson* [1994] and the dimensionless depth, $k_p d$. These parameters yielded similar results to Figure 5.

[35] On the basis of these results, it seems that the harmonic appears quite suddenly with decreasing water depth, presumably when three-wave interactions begin to become important in the source term balance. The exact point where this occurs cannot be determined from the data, but it presumably lies near $k_p d \approx 3$, the deep water limit and the upper bound of the present data set. Once the harmonic is generated, it does not appear to grow with decreasing

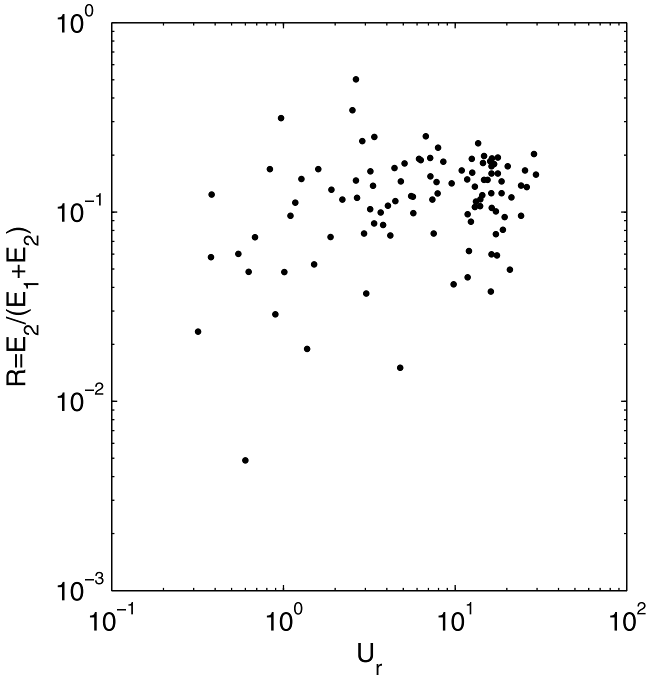

Figure 5. Ratio of the energy in the harmonic peak, E_2, to the total energy of the spectrum, $E_1 + E_2$, as a function of the Ursell parameter, U_r. The full data set of Table 1 is shown.

water depth (increasing nonlinearity), but remains constant at $R \approx 0.05-0.20$.

5.3. Spectral Parameters

[36] In comparison to previous field studies of wind wave spectra, the present study has the advantage of resolving the spectrum to high frequency (12.5 Hz) and with small confidence limits for the spectra (see Figures 4a and 4b). As a result, it is possible to determine the spectral parameters to reasonable confidence. With eight fitting parameters in the spectral form (14), some care needs to be exercised to ensure that unrealistic results do not occur. Initially, the region of the spectrum between $5f_p$ and $10f_p$ was extracted and n_1 and β_1 determined by a simple power law fit to this region. In addition to reducing the number of fitting parameters in the subsequent Levenberg-Marquardt nonlinear regression, it also insured that data close to the Nyquist frequency of 12.5 Hz were excluded (noting the highest values of f_p were approximately 0.9 Hz), thus removing concerns that aliasing may corrupt the results.

[37] Figure 6 shows a plot of $|n_1|$ as a function of the depth parameter, k_pd for the asymptotic depth-limited data set. The mean value of the data is $n_1 = -3.9$, with no obvious trend as a function of k_pd. This result is a little surprising as, on the basis of the theory of *Kitaigorodskii* [1962], *Bouws et al.* [1985] speculated that the universal form for the wave spectrum, irrespective of depth, should be expressed in the wave number form, $F(k) \propto k^{-3}$. This form yields a frequency spectrum of the form, $F(f) \propto f^{-5}$ in deep water and $F(f) \propto f^{-3}$, at the shallow water limit. Noting the increasing observational evidence that deep water spectra are, in fact, proportional to f^{-4} (e.g., *Donelan et al.* [1985], amongst many others), *Miller and Vincent* [1990] proposed that the universal form should be $F(k) \propto k^{-2.5}$, yielding $F(f) \propto f^{-4}$ in deep water and $F(f) \propto f^{-2.5}$ at the shallow water limit. *Young and Verhagen* [1996b] found some evidence for a decrease in the value of the exponent with decreasing water depth, although their data exhibited significant scatter.

[38] Noting that the values of n_1 were obtained in the frequency range $5f_p < f < 10f_p$ and considering the range of values of f_p in the data set, the spectral components in this frequency range are always in deep water. That is, one would not expect any measurable change in the spectral slope as a function of k_pd due to direct interactions of waves from this range of scales with the bottom. The physical reason for a potential change in spectral slope is as a result of a change in the balance of the source terms in the tail of the spectrum, rather than due to a simple scaling relationship. Although this balance is not yet fully understood, Figure 6 indicates that for these asymptotic depth-limited wind wave spectra $n_1 \approx -4$, with no measurable dependence on depth. As noted above, the mean value is actually -3.9. Figure 6 also shows the 95% confidence limit due to the natural sampling variability for the individual data points (approximately ±4 %). This variability accounts for the scatter evident in the data and leads us to conclude that for practical purposes, $n_1 = -4$, with no clear variation with depth.

[39] *Bouws et al.* [1985] and *Young and Verhagen* [1996b] assumed that the shape functions in the spectrum could be disregarded such that $F(k) \propto \beta k^n$ and that the total energy could be approximated by $E = \int_{k_p}^{\infty} k^n dk$. Introducing nondimensional variables, this results in a relationship between ε, κ and β. The present data do support such a

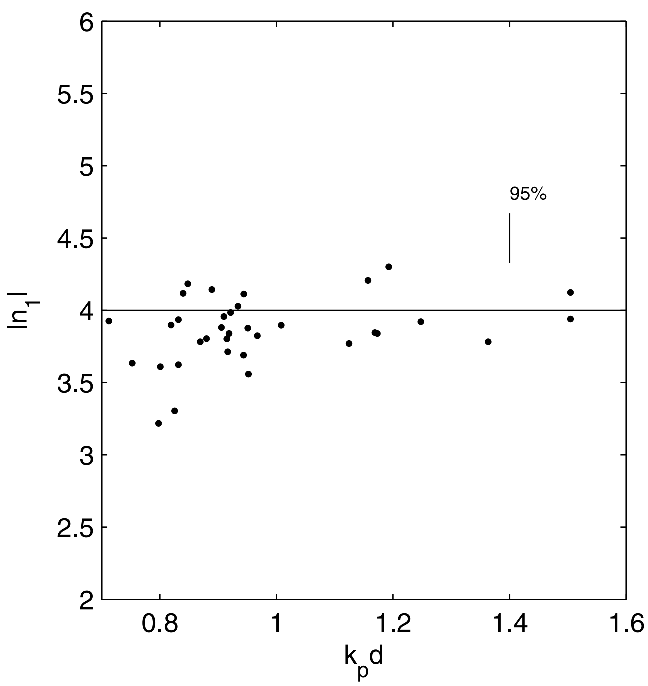

Figure 6. Absolute value of the spectral slope parameter, n_1, as a function of k_pd. Only asymptotic depth-limited data are shown. The horizontal line is drawn at $|n_1| = 4$. The 95% confidence interval, as calculated in Appendix A, for the individual data points is shown by the vertical line.

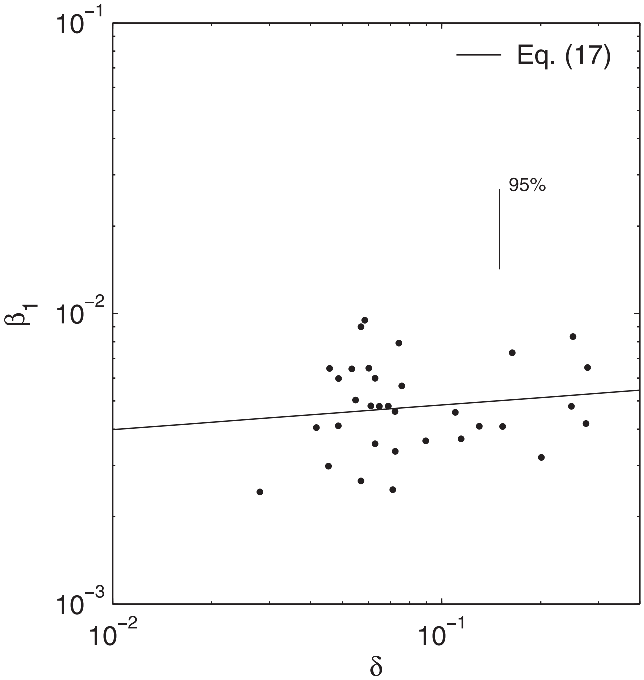

Figure 7. Spectral-scale parameter, β_1, as a function of the nondimensional depth, δ. Only asymptotic depth-limited data are shown. The fit to the data represented by (17) is shown by the solid line. The 95% confidence interval, as calculated in Appendix A, for the individual data points is shown by the vertical line.

relationship between ε, κ and β_1. Both ε and κ are correlated with δ as indicated in Figure 3. Hence it is more logical to investigate the relationship between β_1 and δ, as shown in Figure 7.

[40] There is a correlation between β_1 and δ, with β_1 slowly decreasing with decreasing nondimensional depth. A least squares approximation to the data yields

$$\beta_1 = 5.89 \times 10^{-3}\delta^{0.085} \tag{17}$$

The scatter in the data observed in Figure 7 is consistent with the expected sampling variability shown by the 95% confidence limits for the individual data points (see Appendix A).

[41] A variety of deep water field experiments have attempted to find consistent relationships for the spectral shape parameters γ and σ [e.g., *Hasselmann et al.*, 1973; *Donelan et al.*, 1985]. Although *Donelan et al.* [1985] report some success, such spectral studies have generally not found clear trends for these parameters. Similarly, in finite depth conditions *Bouws et al.* [1985] and *Young and Verhagen* [1996b] could not determine a functional dependence for these parameters. Although it is possible that no such relationships exist, it is likely that the combination of the limitations of an arbitrarily chosen spectral form, together with the sampling variability of the spectrum has masked such a dependence.

[42] In the context of the present data, we searched for a dependence of γ_1 and σ_1 in terms of the other parameters. As shown in Figures 8 and 9, both of these parameters are correlated with β_1. Both γ_1 and σ_1, increase as β_1 decreases, that is, as the nondimensional water depth δ, decreases. Least squares fits to the data yield

$$\gamma_1 = 2.97 \times 10^{-3}\beta_1^{-1.34} \tag{18}$$

$$\sigma_1 = 2.0 \times 10^{-6}\beta_1^{-2.09} \tag{19}$$

As stated previously, a harmonic exists at approximately $2f_p$. A visual examination of the spectra indicates that, in fact, the harmonic is almost always at a frequency less than $2f_p$. Figure 10 shows f_{p_2}/f_{p_1} as a function of k_pd. There is no correlation with k_pd, although values of f_{p_2} range from $1.5f_{p_1}$ to $2.0f_{p_1}$, with a mean value of $f_{p_2} = 1.76f_{p_1}$. The scatter in the values of f_{p_2} are most likely associated with sampling variability. The harmonic peak is generally not a clear sharp peak, often being a broad peak or sometimes simply a change in spectral slope (see Figure 4). As a result, the fitting routine would be expected to yield considerable variability in the resulting values.

[43] The remaining spectral parameters, n_2 and β_2 are not expected to yield consistent functional dependencies, mainly because of the limited energy in the harmonic peak and the challenges of representing this peak with the rather crude form of F_2. It is implicitly assumed that $|n_2| > |n_1|$, such that the component F_2 will not influence the high-frequency spectral tail of the spectrum. The mean values of these

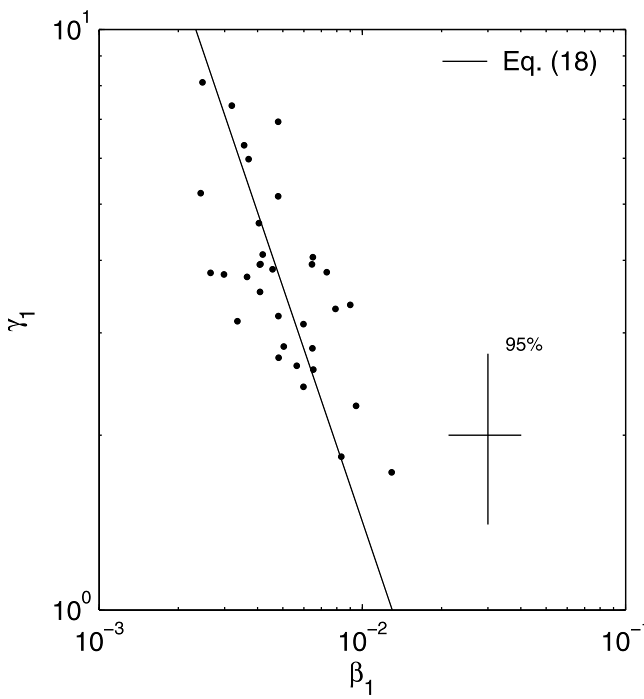

Figure 8. Spectral shape parameter, γ_1, as a function of the scale parameter β_1. Only asymptotic depth-limited data are shown. The fit to the data represented by (18) is shown by the solid line. The 95% confidence intervals, as calculated in Appendix A, for the individual data points are shown by the cross.

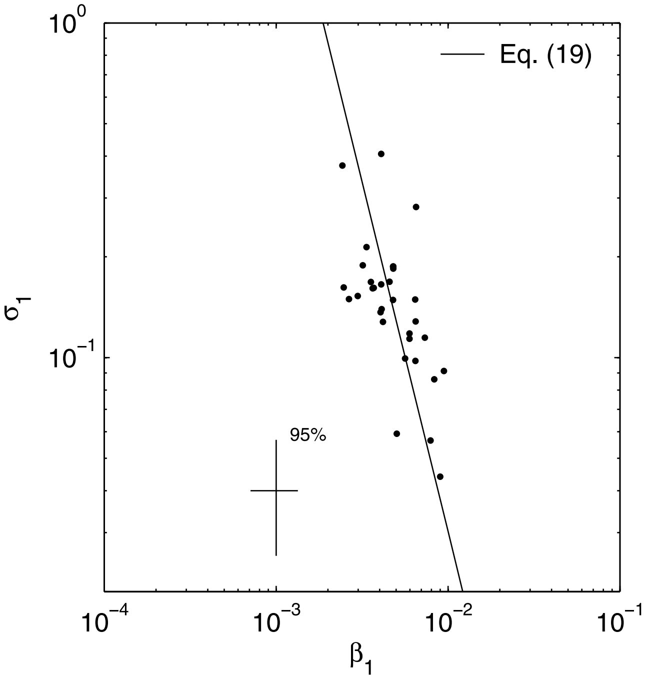

Figure 9. Spectral shape parameter, σ_1, as a function of the scale parameter β_1. Only asymptotic depth-limited data are shown. The fit to the data represented by (19) is shown by the solid line. The 95% confidence intervals, as calculated in Appendix A, for the individual data points are shown by the cross.

quantities were, $n_2 = -8.35$ (i.e., $|n_2| > |n_1|$) and $\beta_2 = 0.074$. These mean values have been adopted for further analysis.

6. Discussion and Conclusions

[44] Equations (10) to (19) represent a system of equations which define the full asymptotic form of the depth-limited frequency spectrum with knowledge of only d and U_{10}. From these two parameters, δ can be determined. With the value of δ, ε_d and hence the total energy (or significant wave height) can be calculated from (10) and κ_d and hence k_{p_1} or f_{p_1} from (12). The values of β_1, γ_1 and σ_1 can be determined from (17), (18) and (19), respectively and n_1 assumed to take a value of -4. The remaining three spectral parameters, n_2, f_{p_2} and β_2 can be approximated by their mean values indicated above. Thus all the parameters in (14) are defined.

[45] The consistency of this set of equations does, however, need to be checked [e.g., *Lewis and Allos*, 1990; *Babanin and Soloviev*, 1998]. As (14) is fully defined, the spectrum can be integrated to determine the total energy, E and hence the nondimensional energy ε. This value should be consistent with the predictions of (10). Figure 11 shows the results of a series of tests where a range of value for d and U_{10} where chosen such as to generate value of δ spanning the range of typical field data. The resulting spectra were then integrated to determine E and ε, and the results compared with (10). The results, as shown in Figure 11 agree well, demonstrating the relationships are self-consistent.

[46] The relationships presented above show that there is not one universal asymptotic depth-limited spectrum. Depth-limited spectra can occur over a very broad range of values of nondimensional depth δ and the spectrum is a function of δ. As δ decreases, β_1 decreases and both γ_1 and σ_1 increase. Hence, as δ decreases, the energy in the high-frequency tail of the spectrum decreases (i.e., $\beta_1 \downarrow$) while the energy near the spectral peak increases (i.e., $\gamma_1 \uparrow$, $\sigma_1 \uparrow$). This behavior is consistent with the limited understanding we have of the source term balance in finite water depth. *Hasselmann and Hasselmann* [1981] have shown that as the water depth decreases the magnitude of the nonlinear four-wave interactions increases. This could be expected to result in an increased energy flux from the high-frequency spectral tail to the peak, consistent with the observed results.

[47] The other significant feature of the spectra reported in this paper is the harmonic at a frequency slightly less than $2f_p$. If not accounted for, this feature may affect estimates of the mean frequency in finite depths. Resonant three-wave or triad interactions can only take place in shallow water, where the waves are nondispersive and colinear [e.g., *Elgar et al.*, 1995; *Young*, 1999]. This occurs since only these components can satisfy the resonant conditions. This would result in a harmonic at $2f_p$. As the conditions reported here are in intermediate water depths, it is unlikely that this is the mechanism responsible for the generation of the harmonic. *Armstrong et al.* [1962], *Freilich and Guza* [1984], and *Elgar et al.* [1993] have, however, shown that significant energy transfers can also occur because of near-resonant interactions, in which the interacting components nearly satisfy the dispersion relationship. Such interactions allow components over a range of wave numbers and directions to interact. This effect may explain why the harmonic peak in the present data is not exactly at $2f_p$. This may also occur because of other source terms such as wind input and four-

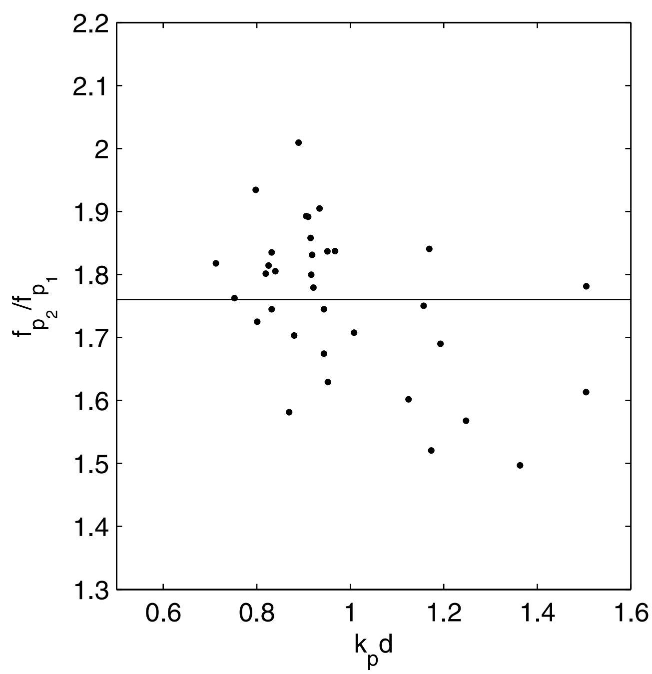

Figure 10. Ratio of the peak frequency of the harmonic, f_{p_2}, to the peak frequency of the spectrum, f_{p_1}, as a function of $k_p d$. Only asymptotic depth-limited data are shown. The horizontal line shows the mean value $f_{p_2}/f_{p_1} = 1.76$.

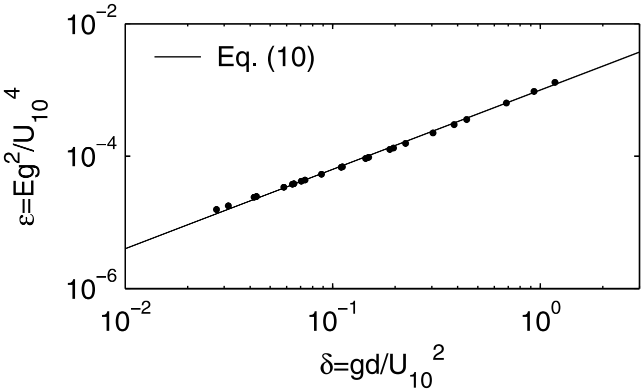

Figure 11. Nondimensional energy, ε, as a function of the nondimensional water depth, δ. The asymptotic limit defined by (10) is shown by the solid line. The dots show quantities calculated for a range of values of U_{10} and d. Parametric forms of the spectra were calculated for these values and were integrated to determine the total energy. The good agreement with (10) demonstrates the self-consistency of the relationships.

wave nonlinear interactions causing further migration of the harmonic to lower frequencies over the extended propagation path of the spectrum.

[48] In contrast to other studies (deep water) of spectral shape, the present results show consistent trends for the spectral shape parameters of γ_1 and σ_1. As shown by the error analysis in Appendix A, these spectral parameters are difficult to estimate from spectra because of the statistical variability of spectral estimates made from finite length time series. The water surface elevation measurements in the present experiments were designed to produce spectra with many degrees of freedom and hence relatively small confidence limits (see Figure 4). Thus the spectral parameters can be determined with a relatively high degree of confidence. The data scatter observed for all parameters is consistent with the confidence limits for these parameters as calculated in Appendix A and shown on the relevant figures.

[49] This paper presents a unique data set clearly defining the form of the asymptotic depth-limited wave spectrum. It should be noted that this is the limiting form which can be generated by the wind in finite depth conditions. It is no doubt possible for waves generated in deep water to propagate to a finite depth site which will not conform to the results presented.

Appendix A: Error Analysis

[50] Each of the spectra used in this study represent one possible realization of the true surface wave spectrum. This occurs because of the fact that the spectrum is calculated from a water surface elevation record of finite length. In the present case, the spectra were calculated from records of 30,000 points, each spectrum being formed by ensemble averaging approximately 117 raw spectra each of 256 points. Hence each spectral ordinate of the final spectrum follows a chi-square probability distribution with 234 degrees of freedom [*Bendat and Piersol*, 1971].

[51] As a result, spectral parameters obtained from the curve fit to the spectrum will also be probabilistic variables. In order to assess the appropriateness of the parameters, it is necessary to understand the confidence limits associated with each of the spectral parameters.

[52] A Monte-Carlo simulation approach was adopted to determine the confidence limits for each of the spectral parameter estimates. A mean spectral form was generated with parameters typical of those measured in this study ($\beta_1 = 5 \times 10^{-3}$, $f_{p_1} = 0.4$ Hz, $\sigma_1 = 0.15$, $\gamma_1 = 3.5$, $n_1 = -4$, $\beta_2 = 7.4 \times 10^{-2}$, $f_{p_2} = 1.75 f_{p_1}$ and $n_2 = -8$). A total of 10,000 realizations of this spectrum were then generated. For each spectrum, each spectral ordinate was allowed to take a random value which satisfied a chi-square probability distribution with 234 degrees of freedom about the spectral ordinate generated by this mean spectrum. The curve fitting routine was then applied to this family of spectra and 10,000 resulting sets of spectral parameter estimates were obtained. The parameter estimates were placed in ascending order and the 0.05 and 0.95 percentage points determined, to estimate the 95% confidence limits.

[53] The resulting confidence limits can be expressed as multiples of the mean values:

$$\beta_{0.05}^{0.95} = \begin{cases} 1.340 \\ 0.709 \end{cases} \beta_1$$

$$f_{p0.05}^{0.95} = \begin{cases} 1.029 \\ 0.971 \end{cases} f_{p_1}$$

$$\sigma_{0.05}^{0.95} = \begin{cases} 1.419 \\ 0.639 \end{cases} \sigma_1$$

$$\gamma_{0.05}^{0.95} = \begin{cases} 1.382 \\ 0.702 \end{cases} \gamma_1$$

$$n_{0.05}^{0.95} = \begin{cases} 1.038 \\ 0.961 \end{cases} n_1$$

As can be seen, the parameters β_1, γ_1 and σ_1 have relatively large confidence intervals, even though the spectra used in this study have small confidence limits. This reflects the large scatter which is typically reported for these parameters.

Appendix B: Examples of the Predictive Capability of the Proposed Parametric Form

[54] In order to provide some indication of the potential accuracy (and consistency) of the parametric relationships proposed, the following test was conducted. For each of the spectra used to develop the relationships, the water depth and wind speed was noted. With these values, the full set of spectral parameters was determined and the resulting parametric form of the spectrum compared to the original data. In all cases, the parametric spectral form and the measured data visually compared well. Typical examples of these results are shown in Figure B1. The four cases shown in Figure B1 represent: c031442.se8 – U_{10} = 5.7 m/s, d = 0.91 m; c031356.se8 – U_{10} = 7.5 m/s, d = 0.94 m; c011323.oc8 – U_{10} = 10.2 m/s, d = 0.95 m; c311845.oc7 – U_{10} = 15.0 m/s, d = 1.04 m.

[55] Although these results are impressive, it should be noted that this is more a consistency test than an objective

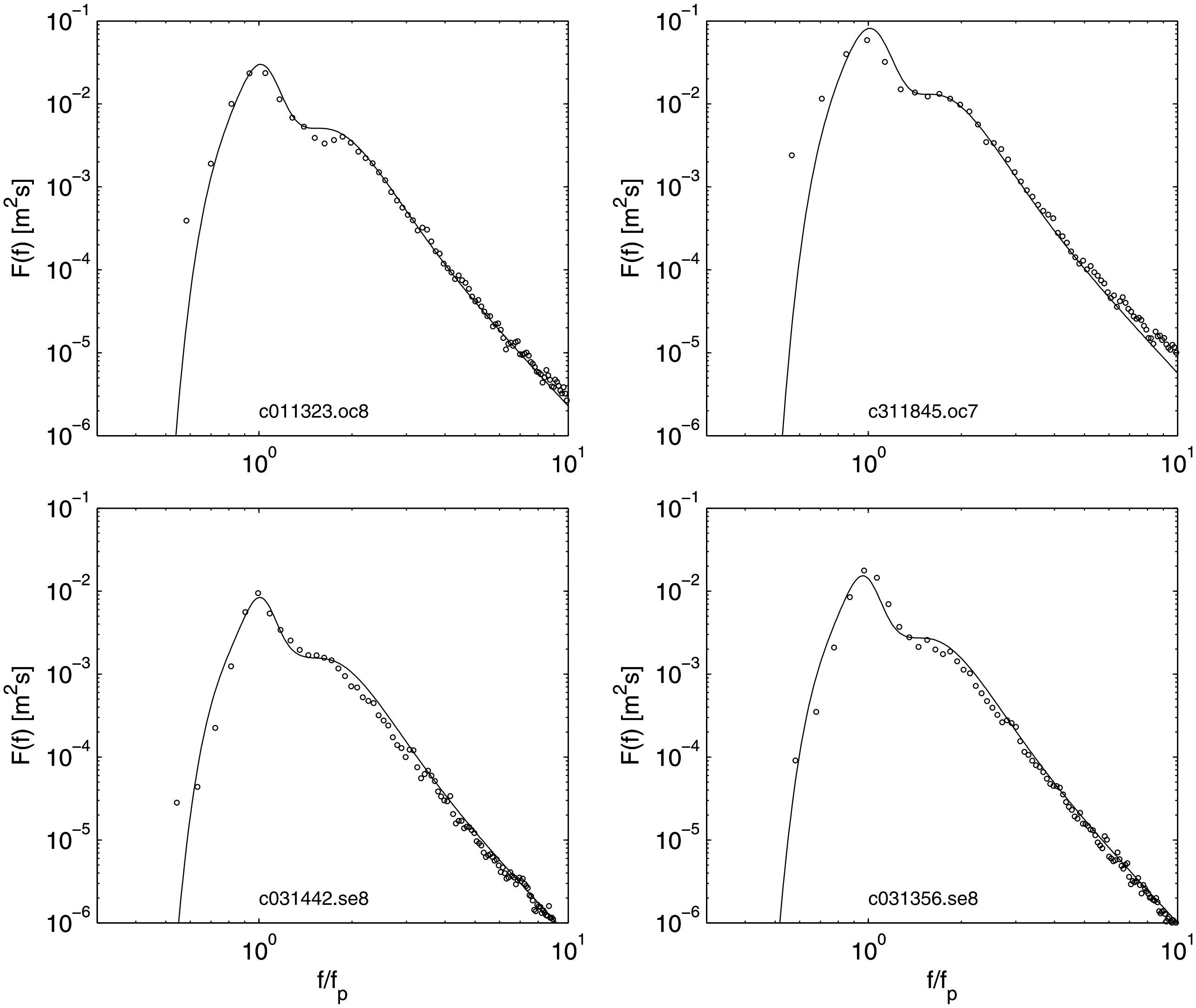

Figure B1. Four examples of spectra calculated using the parametric relationships developed in the paper. The open dots show the recorded spectra. With the measured values U_{10} and d for each of these cases, the parametric form of the spectrum was calculated and is plotted as the solid line. The spectra shown are designated by the reference numbers at the bottom of each plot and can be cross-referenced to Table 1.

measure of accuracy, as the spectra shown in Figure B1 were part of the data set used to generate the functional relationships for the parameters.

[56] **Acknowledgments.** The authors gratefully acknowledge the financial support of the U.S. Office of Naval Research (grants N00014-97-1-0234, N00014-97-*1*-0277, and N0014-97-1-0233) and the Australian Research Council (grant A00102965). We also express our gratitude to the staff and students of the School of Civil Engineering of the Australian Defence Force Academy: Jim Baxter, Karl Shaw, Ian Shephard, and Michael Wilson, who offered highly professional and prompt responses to all urgent demands during the experiments. We are also very grateful to CSIRO, Canberra, and the School of Aerospace and Mechanical Engineering, ADFA, for their assistance with calibrations of the wind sensors.

References

Armstrong, J. A., N. Bloembergen, J. Ducuing, and P. S. Pershan (1962), Interactions between light waves in a nonlinear dielectric, *Phys. Rev.*, *127*, 1918–1939.

Babanin, A. V., and Y. P. Soloviev (1998), Field investigation of transformation of the wind wave frequency spectrum with fetch and the stage of development, *J. Phys. Oceanogr.*, *28*, 563–576.

Battjes, J. A., T. F. Zitman, and L. H. Holthuijsen (1987), A reanalysis of the spectra observed in JONSWAP, *J. Phys. Oceanogr.*, *17*, 1288–1295.

Beji, S., and J. A. Battjes (1993), Experimental investigation of wave propagation over a bar, *Coastal Eng.*, *19*, 151–162.

Bendat, J. S., and A. G. Piersol (1971), *Random Data: Analysis and Measurement Procedures*, 407 pp., John Wiley, Hoboken, N. J.

Bouws, E., H. Günther, W. Rosenthal, and C. L. Vincent (1985), Similarity of the wind wave spectrum in finite depth water: 1. Spectral form, *J. Geophys. Res.*, *90*, 975–986.

Bouws, E., H. Günther, W. Rosenthal, and C. L. Vincent (1987), Similarity of the wind wave spectrum in finite depth water: 2. Statistical relationships between shape and growth stage parameters, *Dtsch. Hydrogr. Z.*, *40*, 1–24.

Bretschneider, C. L. (1958), Revisions in wave forecasting: Deep and shallow water, paper presented at 2nd Conference on Coastal Engineering, Counc. on Wave Res., Am. Soc. Of Civ. Eng., Houston, Tex.

Coastal Engineering Research Center (1984), Shore protection manual, U.S. Army Coastal Eng. Res. Cent., Vicksburg, Miss.

Donelan, M. A., J. Hamilton, and W. H. Hui (1985), Directional spectra of wind-generated waves, *Philos. Trans. R. Soc. London, Ser. A*, *315*, 509–562.

Eldeberky, Y., and J. A. Battjes (1995), Parameterization of triad interactions in wave energy models, in *Coastal Dynamics '95*, edited by W. R. Dally and R. B. Zeidler, pp. 140–148, Am. Soc. of Civ. Eng., Reston, Va.

Elgar, S., R. T. Guza, and M. H. Freilich (1993), Observations of nonlinear interactions in directionally spread shoaling surface gravity waves, *J. Geophys. Res.*, *98*, 20,299–20,305.

Elgar, S., T. H. C. Herbers, V. Chandran, and R. T. Guza (1995), Higher-order spectral analysis of nonlinear ocean surface gravity waves, *J. Geophys. Res.*, *100*, 4977–4983.

Forristall, G. Z. (1981), Measurements of a saturation range in ocean wave spectra, *J. Geophys. Res.*, *86*, 8075–8084.

Freilich, M. H., and R. T. Guza (1984), Nonlinear effects on shoaling surface gravity waves, *Philos. Trans. R. Soc. London, Ser. A*, *311*, 1–41.

Hasselmann, K., et al. (1973), Measurements of wind-wave growth and swell decay during the Joint North Sea Wave Project (JONSWAP), *Dtsch. Hydrogr. Z., Suppl. A*, *8*, 1–95.

Hasselmann, S., and K. Hasselmann (1981), A symmetrical method of computing the nonlinear transfer in a gravity wave spectrum, *Hamburg. Geophys. Einzelschr., Ser. A*, *52*, 1–138.

Hasselmann, S., and K. Hasselmann (1985), Computations and parameterizations of the nonlinear energy transfer in a gravity wave spectrum. part 1: A new method for efficient computations of the exact nonlinear transfer integral, *J. Phys. Oceanogr.*, *15*, 1369–1377.

Ijima, T., and F. L. W. Tang (1966), Numerical calculations of wind waves in shallow water, paper presented at 10th Conference on Coastal Engineering, Am. Soc. of Civ. Eng., Tokyo.

Kahma, K. K. (1981), A study of the growth of the wave spectrum with fetch, *J. Phys. Oceanogr.*, *11*, 1503–1515.

Kahma, K. K., and C. J. Calkoen (1992), Reconciling discrepancies in the observed growth of wind-generated waves, *J. Phys. Oceanogr.*, *22*, 1389–1405.

Kawai, S., K. Okada, and Y. Toba (1977), Field data support of three-seconds law and $gu_*\sigma^{-4}$ spectral form for growing wind waves, *J. Oceanogr. Soc. Jpn.*, *33*, 137–150.

Kitaigorodskii, S. A. (1962), Applications of the theory of similarity to the analysis of wind-generated wave motion as a stochastic process, *Bull. Acad. Sci. USSR Geophys. Ser.*, *1*, 105–117.

Kitaigorodskii, S. A., V. P. Krasitskii, and M. M. Zaslavskii (1975), On Phillips' theory of equilibrium range in the spectra of wind-generated gravity waves, *J. Phys. Oceanogr.*, *5*, 410–420.

Komen, G. J., L. Cavaleri, M. Donelan, K. Hasselmann, S. Hasselmann, and P. A. E. M. Janssen (1994), *Dynamics and Modelling of Ocean Waves*, 532 pp., Cambridge Univ. Press, New York.

Levenberg, K. (1944), A method for the solution of certain problems in least squares, *Q. Appl. Math.*, *2*, 164–168.

Lewis, A. W., and R. N. Allos (1990), JONSWAP's parameters: Sorting out inconsistencies, *Ocean Eng.*, *17*, 409–415.

Miller, H. C., and C. L. Vincent (1990), FRF spectrum: TMA with Kitaigorodskii's f^{-4} scaling, *J. Waterw. Port Coastal Ocean Eng.*, *116*, 57–78.

Mitsuyasu, H., F. Tasai, T. Suhara, S. Mizuno, M. Onkusu, T. Honda, and K. Rukiiski (1980), Observations of the power spectrum of waves using a cloverleaf buoy, *J. Phys. Oceanogr.*, *10*, 286–296.

Nelson, R. C. (1994), Depth limited design wave heights in very flat regions, *Coastal Eng.*, *23*, 43–59.

Smith, J. M., and C. L. Vincent (2002) Application of spectral equilibrium ranges in the surf zone, paper presented at 28th International Coastal Engineering Conference, Am. Soc. of Civ. Eng., Cardiff, U. K.

Thijsse, J. T. (1949), Dimensions of wind-generated waves, paper presented at General Assembly of Association d'Océanographie Physique, Oslo.

Toba, Y. (1973), Local balance in the air-sea boundary process, *J. Oceanogr. Soc. Jpn.*, *29*, 209–220.

Tozer, N. P., K. Millard, and A. Saulter (2005) Validation issues for a global coastal wave forecast system, *Pap. 210*, in *Proceedings of Ocean Waves Measurement and Analysis, 5th International Symposium WAVES2005, 3–7 July, Madrid, Spain*, edited by B. Edge and J. C. Santas, Am. Soc. of Civ. Eng., Reston, Va.

U.S. Army Corps of Engineers (1955), Waves and wind tides in shallow lakes and reservoirs, *Summary Rep.*, *Proj. CW-167*, Jacksonville, Fla.

Young, I. R. (1999), *Wind Generated Ocean Waves*, 306 pp., Elsevier, New York.

Young, I. R., and Y. Eldeberky (1998), Observations of triad coupling of finite depth wind-waves, *Coastal Eng.*, *33*, 137–154.

Young, I. R., and G. P. van Vledder (1993), The central role of nonlinear interactions in wind-wave evolution, *Philos. Trans. R. Soc. London, Ser. A*, *342*, 505–524.

Young, I. R., and L. A. Verhagen (1996a), The growth of fetch limited waves in water of finite depth. part I: Total energy and peak frequency, *Coastal Eng.*, *28*, 47–78.

Young, I. R., and L. A. Verhagen (1996b), The growth of fetch limited waves in water of finite depth. part II: Spectral evolution, *Coastal Eng.*, *28*, 79–100.

Young, I. R., L. A. Verhagen, and S. K. Khatri (1996), The growth of fetch limited waves in water of finite depth. part III: Directional spectra, *Coastal Eng.*, *28*, 101–122.

Young, I. R., M. L. Banner, M. A. Donelan, A. V. Babanin, W. K. Melville, F. Vernon, and C. McCormick (2005), An integrated system for the study of wind wave source terms in finite depth water, *J. Atmos. Oceanic Technol.*, *22*(7), 814–828.

Zakharov, V. E. (2005), Theoretical interpretation of fetch limited wind-driven sea observations, *Nonlinear Processes Geophys.*, *12*, 1011–1020.

A. V. Babanin and I. R. Young, Swinburne University of Technology, P.O. Box 218, Melbourne, Vic 3122, Australia. (iyoung@swin.edu.au)